

Applications of computation in acoustics: Ultrasound bioeffects and transmission loss uncertainty

Brandon Patterson

Scientific Computing and Flow Physics Lab

University of Michigan, Ann Arbor

¹Department of Mechanical Engineering

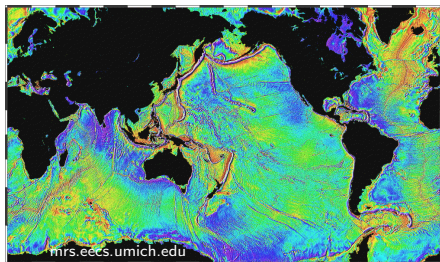
August 10, 2016



Part I: Past Work

Two very different problems in computational acoustics

Acoustic uncertainty in the ocean



Ultrasound bioeffects



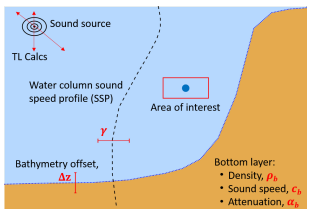
Past work: Efficient estimation of the probability density function of transmission loss in uncertain ocean environments

Transmission Loss, $TL = 20 \log_{10} \left(\frac{P_{source}}{P_{receiver}} \right)$, is useful for naval applications.

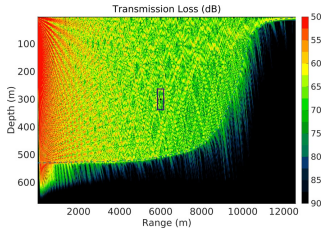
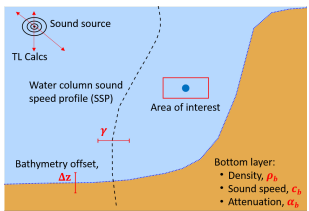


TL uncertainty is important for those making decisions based on TL, but traditional methods are slow and expensive.

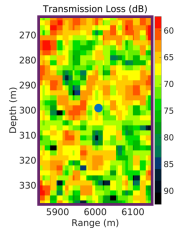
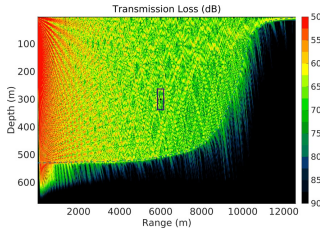
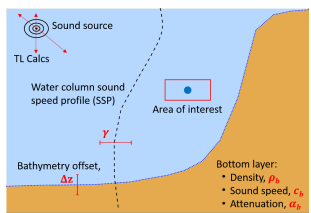
Past work: We developed a computationally efficient way of computing TL in uncertain environments



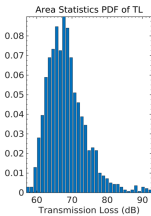
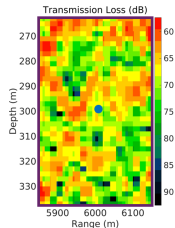
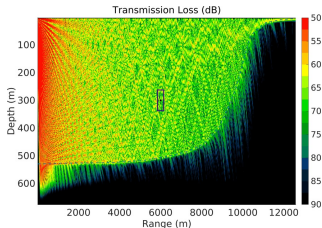
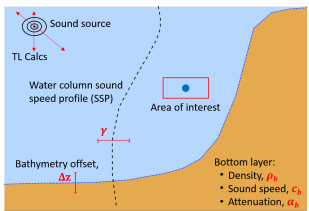
Past work: We developed a computationally efficient way of computing TL in uncertain environments



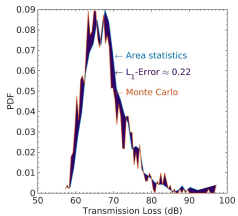
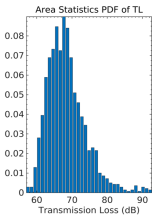
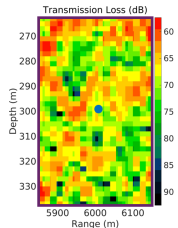
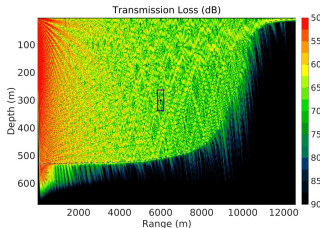
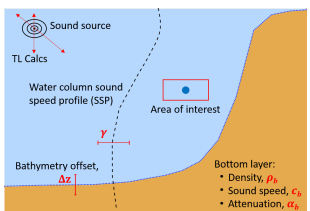
Past work: We developed a computationally efficient way of computing TL in uncertain environments



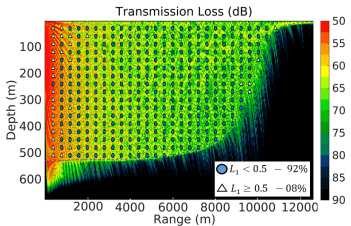
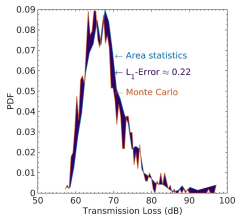
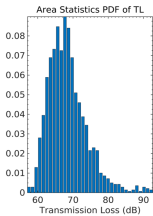
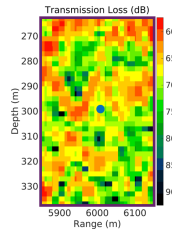
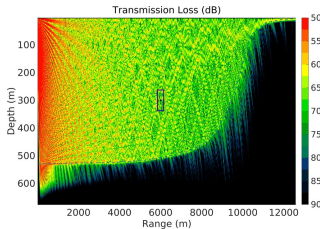
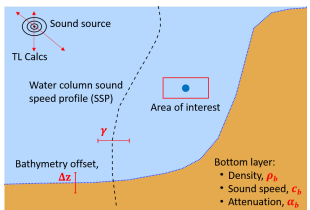
Past work: We developed a computationally efficient way of computing TL in uncertain environments



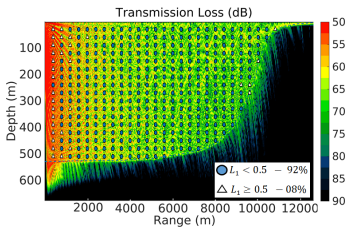
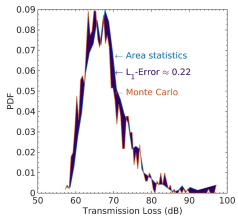
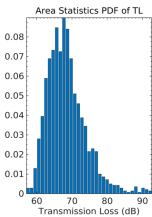
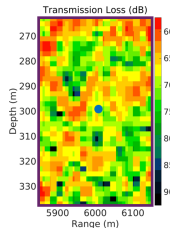
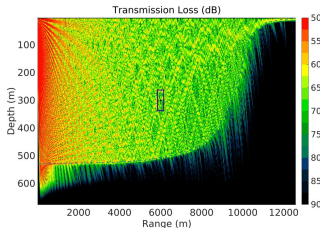
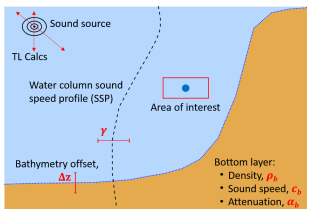
Past work: We developed a computationally efficient way of computing TL in uncertain environments



Past work: We developed a computationally efficient way of computing TL in uncertain environments



Past work: We developed a computationally efficient way of computing TL in uncertain environments



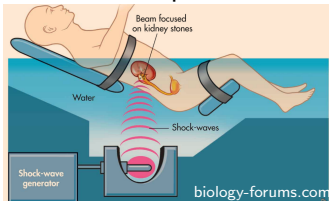
- Engineering level accurate (L_1 -error < 0.5) in 93% of test cases in bottom reflecting environments.
- $\approx \mathcal{O}(10^{-6})$ the cost of 1000-sample Monte Carlo Methods.

Background on medical ultrasound

Diagnostic



Therapeutic



- High frequency (MHz) sound waves travel into the body and scatter at material interfaces.
- Acoustic energy is converted to kinetic via cavitation or dissipated as heat.

Background on medical ultrasound

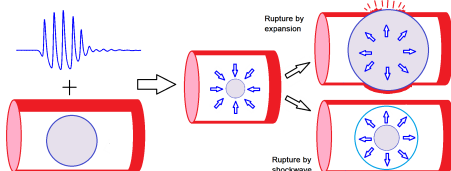
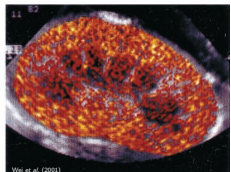
Diagnostic



- High frequency (MHz) sound waves travel into the body and scatter at material interfaces.
- Acoustic energy is converted to kinetic via cavitation or dissipated as heat.

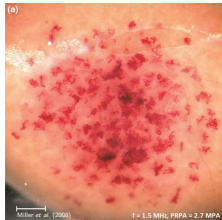
I focus on Diagnostic Ultrasound (DUS) bioeffects and relevant physics.

Background on DUS bioeffects



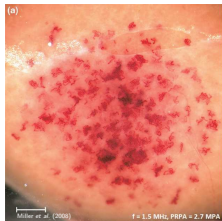
- Diagnostic Ultrasound (DUS) is ubiquitous and generally very safe.
- CEUS uses echogenic microbubbles for contrast, but these may act as cavitation nuclei and can lead to hemorrhage.
- Lung Hemorrhage (LH) is the only known bioeffect of non-contrast diagnostic ultrasound under clinically safe conditions.

Past work: Theoretical microbubble dynamics in a viscoelastic medium at capillary breaching thresholds



Patterson, B., Miller, D. L., & Johnsen, E. (2012). Theoretical microbubble dynamics in a viscoelastic medium at capillary breaching thresholds. JASA, 132(6), 3770.

Past work: Theoretical microbubble dynamics in a viscoelastic medium at capillary breaching thresholds



$$\left(1 - \frac{\dot{R}}{C}\right) R \ddot{R} + \frac{3}{2} \left(1 - \frac{\dot{R}}{3C}\right) \dot{R}^2 = \left(1 + \frac{\dot{R}}{C}\right) \left[p_B - 1 - p_a - \frac{R}{C} \frac{dp_a}{dt} \right] + \frac{R}{C} \dot{p}_B,$$
$$p_B = \left(1 + \frac{2}{We}\right) \frac{1}{R^{3\gamma}} - \frac{2}{WeR} + \tau_R,$$

Patterson, B., Miller, D. L., & Johnsen, E. (2012). Theoretical microbubble dynamics in a viscoelastic medium at capillary breaching thresholds. JASA, 132(6), 3770.

Past work: Theoretical microbubble dynamics in a viscoelastic medium at capillary breaching thresholds



$$\left(1 - \frac{\dot{R}}{C}\right) R \ddot{R} + \frac{3}{2} \left(1 - \frac{\dot{R}}{3C}\right) \dot{R}^2 = \left(1 + \frac{\dot{R}}{C}\right) \left[p_B - 1 - p_a - \frac{R}{C} \frac{dp_a}{dt} \right] + \frac{R}{C} \dot{p}_B,$$
$$p_B = \left(1 + \frac{2}{We}\right) \frac{1}{R^{3\gamma}} - \frac{2}{WeR} + \tau_R,$$

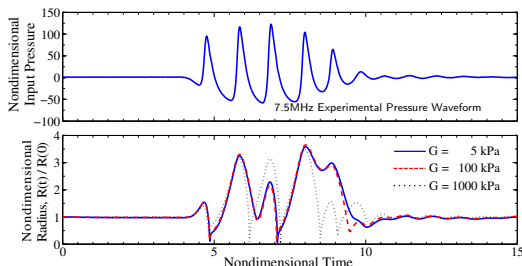
Parameter	Dimensional value	Dimensionless number
Viscosity	$\mu = 0.015 \text{ (Pa s)}$	$\Rightarrow Re = \rho u R_o / \mu = 2/3$
Elasticity	$G = 10^5 \text{ (Pa)}$	$\Rightarrow Ca = \rho u^2 / G = 1.0$
Surface tension	$S = 0.056 \text{ (N/m)}$	$\Rightarrow We = \rho u^2 R_o / S = 2$
Sound speed	$c = 1570 \text{ (m/s)}$	$\Rightarrow C = c/u = 157$

Past work: Theoretical microbubble dynamics in a viscoelastic medium at capillary breaching thresholds



$$\left(1 - \frac{\dot{R}}{C}\right) R \ddot{R} + \frac{3}{2} \left(1 - \frac{\dot{R}}{3C}\right) \dot{R}^2 = \left(1 + \frac{\dot{R}}{C}\right) \left[p_B - 1 - p_a - \frac{R}{C} \frac{dp_a}{dt}\right] + \frac{R}{C} \dot{p}_B,$$
$$p_B = \left(1 + \frac{2}{We}\right) \frac{1}{R^{3\gamma}} - \frac{2}{WeR} + \tau_R,$$

Parameter	Dimensional value	Dimensionless number
Viscosity	$\mu = 0.015 \text{ (Pa s)}$	$\rightarrow Re = \rho u R_o / \mu = 2/3$
Elasticity	$G = 10^5 \text{ (Pa)}$	$\rightarrow Ca = \rho u^2 / G = 1.0$
Surface tension	$S = 0.056 \text{ (N/m)}$	$\rightarrow We = \rho u^2 R_o / S = 2$
Sound speed	$c = 1570 \text{ (m/s)}$	$\rightarrow C = c/u = 157$



Patterson, B., Miller, D. L., & Johnsen, E. (2012). Theoretical microbubble dynamics in a viscoelastic medium at capillary breaching thresholds. JASA, 132(6), 3770.

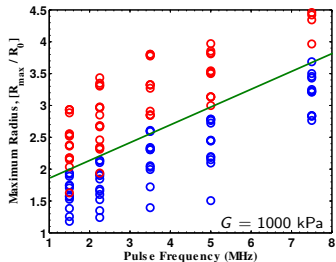
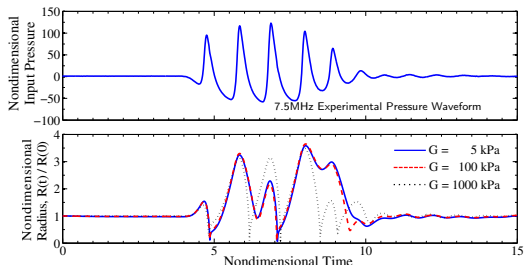
Past work: Theoretical microbubble dynamics in a viscoelastic medium at capillary breaching thresholds



$$\left(1 - \frac{\dot{R}}{C}\right) R \ddot{R} + \frac{3}{2} \left(1 - \frac{\dot{R}}{3C}\right) \dot{R}^2 = \left(1 + \frac{\dot{R}}{C}\right) \left[p_B - 1 - p_a - \frac{R}{C} \frac{dp_a}{dt}\right] + \frac{R}{C} \dot{p}_B,$$

$$p_B = \left(1 + \frac{2}{We}\right) \frac{1}{R^{3\gamma}} - \frac{2}{WeR} + \tau_R,$$

Parameter	Dimensional value	Dimensionless number
Viscosity	$\mu = 0.015 \text{ (Pa s)}$	$\rightarrow Re = \rho u R_o / \mu = 2/3$
Elasticity	$G = 10^5 \text{ (Pa)}$	$\rightarrow Ca = \rho u^2 / G = 1.0$
Surface tension	$S = 0.056 \text{ (N/m)}$	$\rightarrow We = \rho u^2 R_o / S = 2$
Sound speed	$c = 1570 \text{ (m/s)}$	$\rightarrow C = c/u = 157$



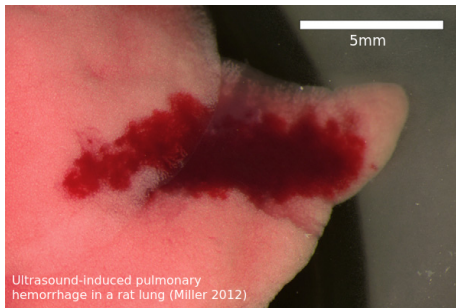
Patterson, B., Miller, D. L., & Johnsen, E. (2012). Theoretical microbubble dynamics in a viscoelastic medium at capillary breaching thresholds. JASA, 132(6), 3770.

Part II: Current Project

Diagnostic ultrasound-induced lung hemorrhage and acoustic wave interactions with liquid-gas interfaces

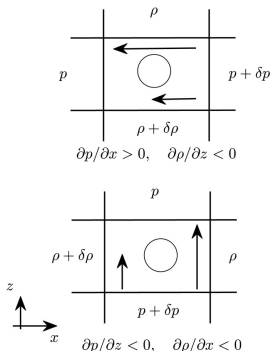
DUS-induced lung hemorrhage is not a new problem

- Lung Hemorrhage (LH) is the only known bioeffect of non-contrast DUS
- Has been shown to occur in mice, rats, pigs, rabbits, monkeys (Child *et al.*, 1990; O'Brien & Zachary, 1997; Tarantal & Canfield, 1994).
- DUS-induced LH does not appear to be a result of cavitation or heating.
- The underlying physical damage mechanism is not understood.

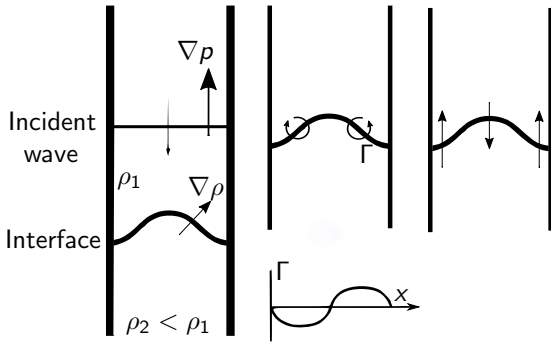


The basic physical problem we have in the lungs is a mechanical wave interacting with an air-tissue interface.

Shock-driven fluid-fluid interfaces have been studied extensively



Adapted from Heifetz & Mak (2015)



Adapted from Brouillette (2002)

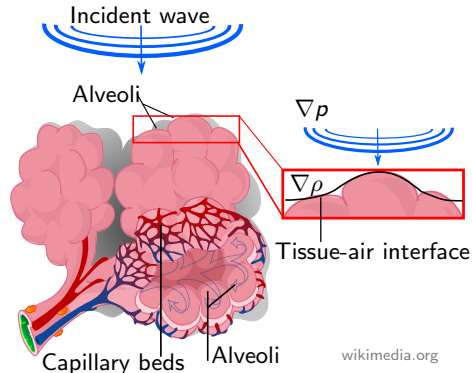
- Shocks deposit baroclinic vorticity at perturbed fluid-fluid interfaces (Drake, 2006).
- This vorticity drives the interface perturbation to grow.
- This is the Richtmyer-Meshkov “instability”.
- Acoustic waves are different. They interact over a finite time-scale.

We aim to use fluid mechanics with computational modeling and simulations to investigate the underlying physics of DUS-lung interaction:

Acoustic wave interactions with liquid-gas interfaces.

We hypothesize that US waves generate baroclinic vorticity at air-tissue interfaces in the lungs, straining fragile alveolar walls.

- Alveolar air-tissue interfaces have sharp density gradients
- US has strong pressure gradients
- US-induced baroclinic vorticity may cause strain, similar to shock-driven interfaces
- Linear acoustics does not capture this.



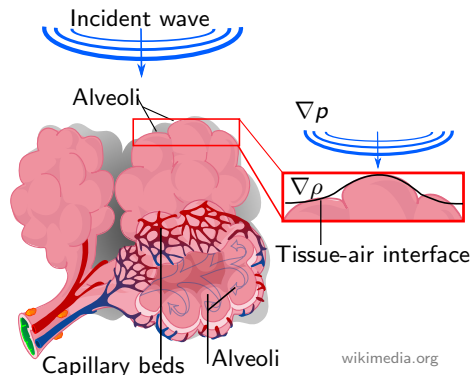
wikimedia.org

We hypothesize that US waves generate baroclinic vorticity at air-tissue interfaces in the lungs, straining fragile alveolar walls.

The vorticity generation equation

$$\frac{\partial \omega}{\partial t} + (\mathbf{u} \cdot \nabla) \omega = (\omega \cdot \nabla) \mathbf{u} - \omega (\nabla \cdot \mathbf{u}) + \frac{\nabla \rho \times \nabla p}{\rho^2} - \nabla \times \left(\frac{\nabla \cdot \boldsymbol{\tau}}{\rho} \right) + \nabla \times \mathbf{B}$$

- Alveolar air-tissue interfaces have sharp density gradients
- US has strong pressure gradients
- US-induced baroclinic vorticity may cause strain, similar to shock-driven interfaces
- Linear acoustics does not capture this.



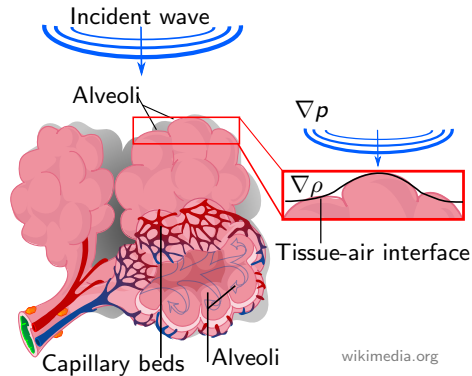
wikimedia.org

We hypothesize that US waves generate baroclinic vorticity at air-tissue interfaces in the lungs, straining fragile alveolar walls.

The vorticity generation equation

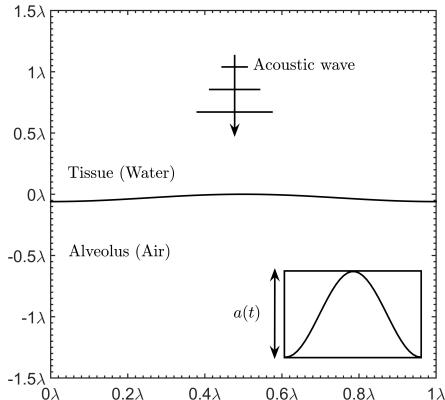
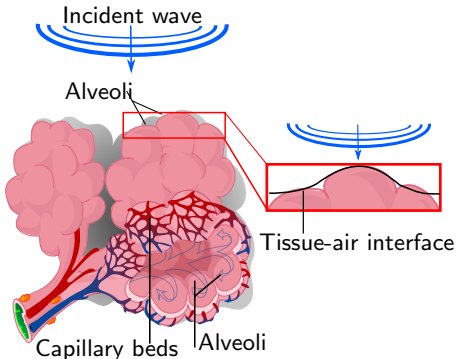
$$\frac{\partial \omega}{\partial t} + (\mathbf{u} \cdot \nabla) \omega = (\omega \cdot \nabla) \mathbf{u}^0 - \omega (\nabla \cdot \mathbf{u}) + \frac{\nabla p \times \nabla p}{\rho^2} - \nabla \times \left(\frac{\nabla p}{\rho} \right)^0 + \nabla \times \mathbf{B}^0$$

- Alveolar air-tissue interfaces have sharp density gradients
- US has strong pressure gradients
- US-induced baroclinic vorticity may cause strain, similar to shock-driven interfaces
- Linear acoustics does not capture this.



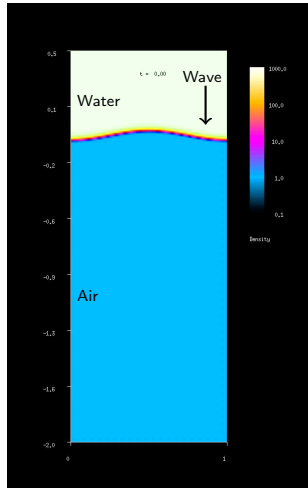
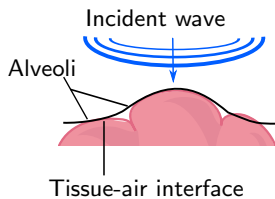
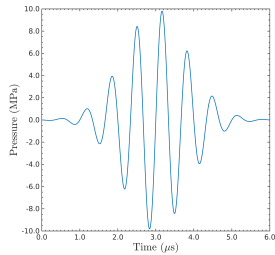
wikimedia.org

Problem setup: We model the ultrasound-alveolar interaction as a 2D, compressible, inviscid fluid system.

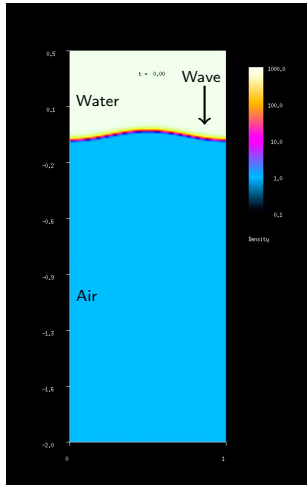
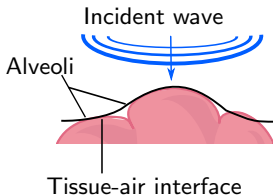
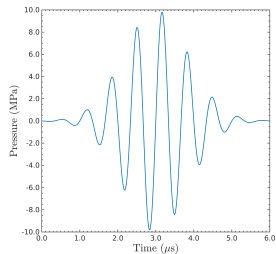


An acoustic wave impinges downward from water toward a perturbed air interface ($a_0=0.06\lambda$).

We simulated and US-pulse impinging on a water-air interface

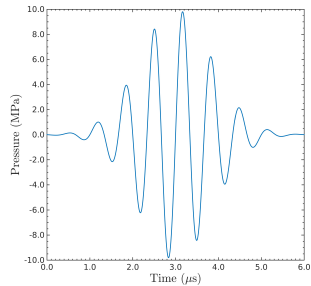


We simulated and US-pulse impinging on a water-air interface

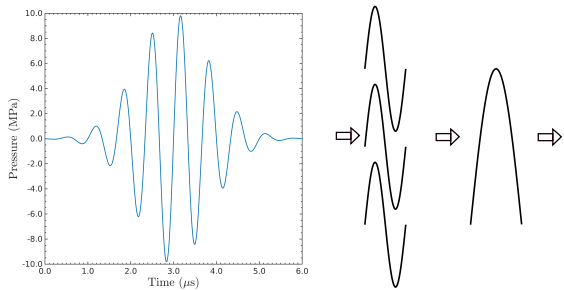


- Linear acoustics doesn't explain the interface deformation.
- The DUS pulse is complicated and not ideal for analysis.

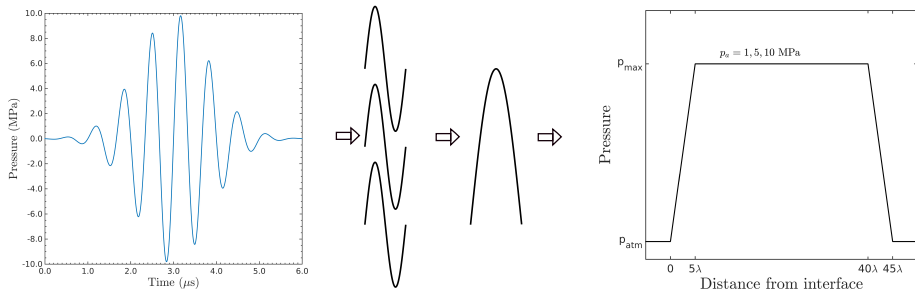
US pulse and Trapezoidal acoustic waveforms are used.



US pulse and Trapezoidal acoustic waveforms are used.



US pulse and Trapezoidal acoustic waveforms are used.



- The trapezoidal waves is simple for understanding physics and analysis, but able to capture feature of US pulse.
- Pulse waveforms are used to check relevance to DUS.

Governing Equations

Euler equations of fluid motion

$$\frac{\partial \rho}{\partial t} + \frac{\partial (\rho u)}{\partial x} + \frac{\partial (\rho v)}{\partial y} = 0,$$

$$\frac{\partial \rho u}{\partial t} + \frac{\partial}{\partial x} \left(\rho u^2 + p \right) + \frac{\partial}{\partial y} (\rho uv) = 0,$$

$$\frac{\partial \rho v}{\partial t} + \frac{\partial}{\partial x} (\rho uv) + \frac{\partial}{\partial y} \left(\rho v^2 + p \right) = 0,$$

$$\frac{\partial E}{\partial t} + \frac{\partial}{\partial x} [u(E + p)] + \frac{\partial}{\partial y} [v(E + p)] = 0,$$

Stiffened equation of state

$$E = \frac{\rho(u^2 + v^2)}{2} + \frac{p + \gamma B}{\gamma - 1}.$$

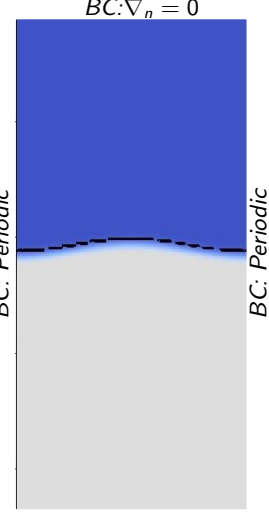
Advection equations for γ, B prevent interface pressure oscillations.

$$\frac{\partial}{\partial t} \left(\frac{\gamma B}{\gamma - 1} \right) + u \frac{\partial}{\partial x} \left(\frac{\gamma B}{\gamma - 1} \right) + v \frac{\partial}{\partial y} \left(\frac{\gamma B}{\gamma - 1} \right) = 0,$$

$$\frac{\partial}{\partial t} \left(\frac{1}{\gamma - 1} \right) + u \frac{\partial}{\partial x} \left(\frac{1}{\gamma - 1} \right) + v \frac{\partial}{\partial y} \left(\frac{1}{\gamma - 1} \right) = 0$$

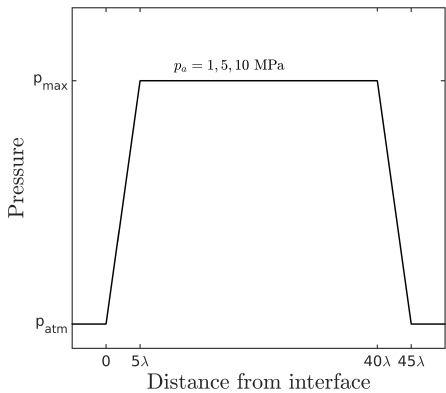
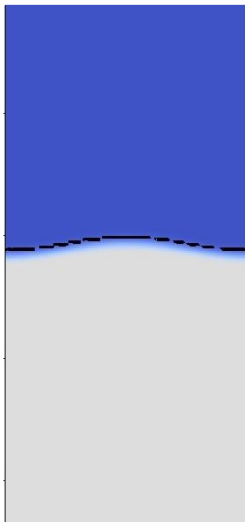
A high-order accurate computational solution strategy is invoked

- An in-house developed code is used to solve the Euler equations.
- Numerical methods
 - 3rd order Discontinuous Galerkin method is used in space
 - 4th order Runge-Kutta time marching
 - Roe Solver used to handle discontinuities
- Acoustic waves are prescribed within the domain.
- Grid stretching reduces reflections.
- Grid size: $\lambda \times 70\lambda (L_x \times L_y)$

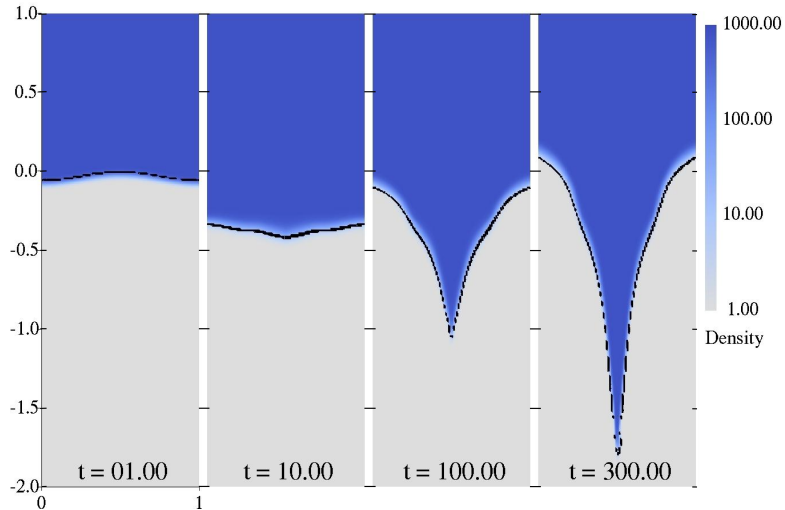


$$BC: \nabla_n = 0$$

Base case: a 10 MPa trapezoidal wave hits the sinusoidal interface

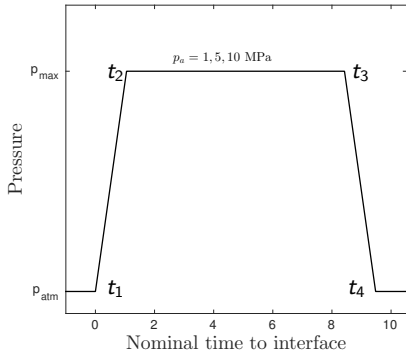
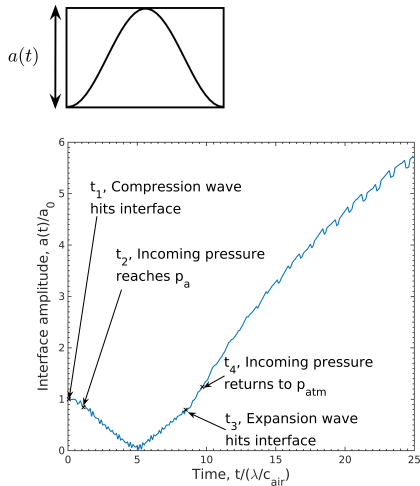


Results: Evolution of the interface after 10 MPa trapezoidal wave



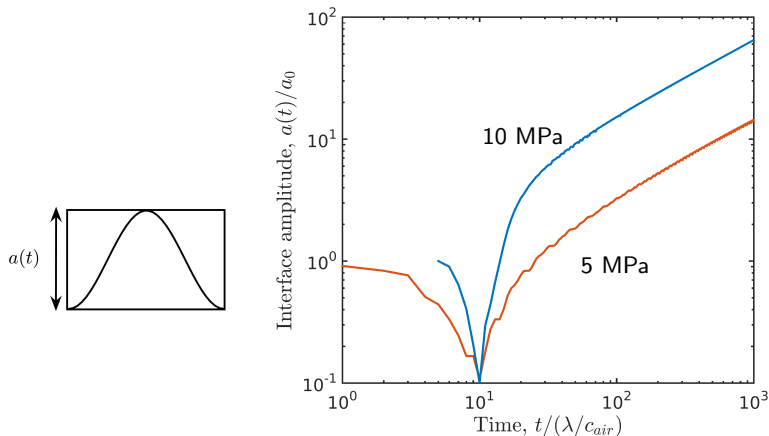
The interface perturbation evolves from a smooth sinusoid into a sharp point.

Results: Early evolution of the interface



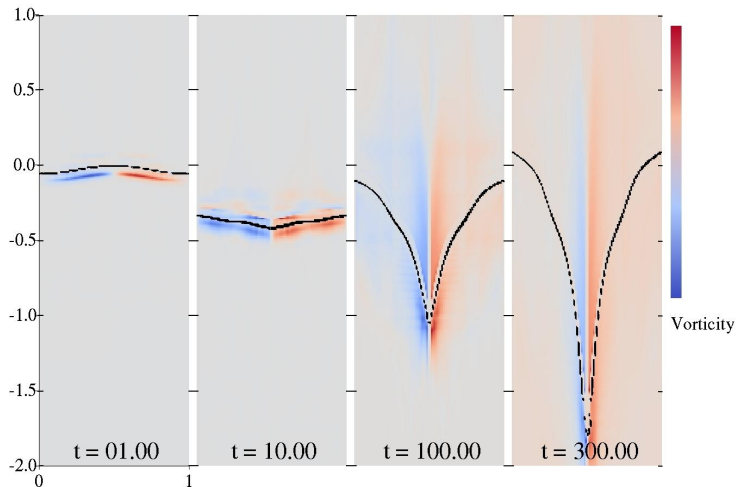
The interface perturbation is initially compressed ($0^+ \leq t \leq 5$), experiences a phase change ($t = 5$), then grows $t > 5$.

Results: Late-time evolution of the interface



We suspect vorticity is driving this late time growth.

Results: Vorticity dynamics for the 10 MPa trapezoidal wave

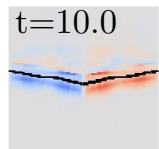
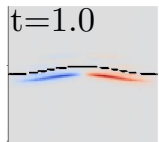
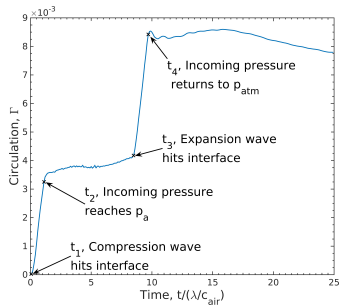
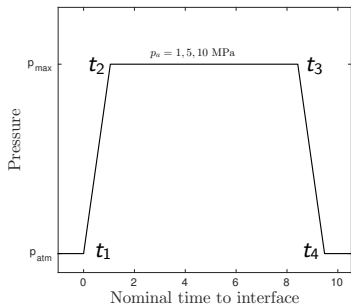


- Vorticity initially deposits in air-dominated ($y_0 < 0.5$) fluid of the interface.
- As the interface evolves, some vorticity advects with it.

Results: A closer look at how circulation is deposited.

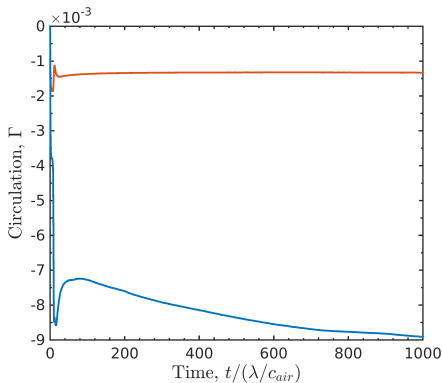
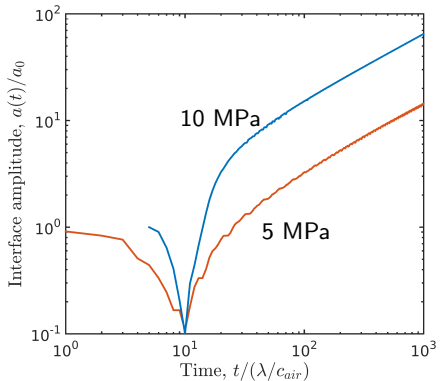
Circulation,

$$\Gamma = \int_{-\infty}^{+\infty} \int_{0.5\lambda}^{1\lambda} \omega \, dx \, dy$$



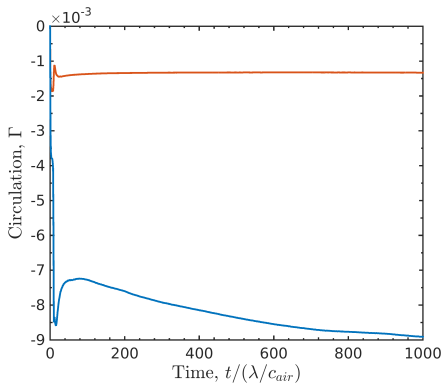
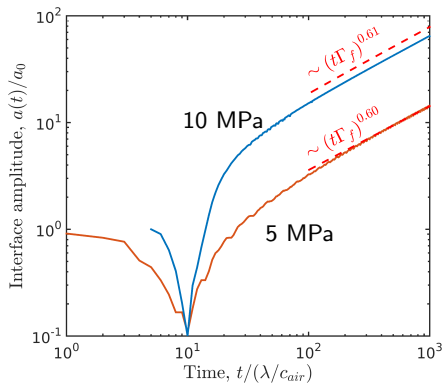
- Both the compression and expansion deposit vorticity.

Results: Late-time evolution of the interface



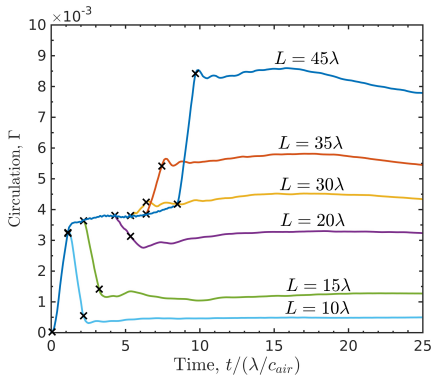
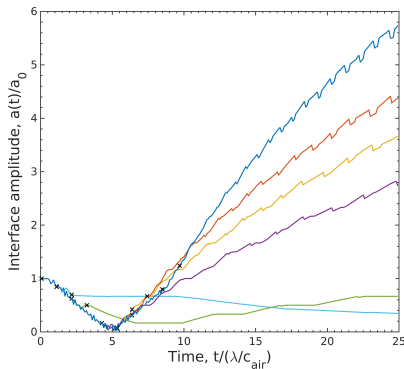
From dimensional analysis, we expect a purely circulation growth of the interface perturbation to behave according to $a(t) \sim \sqrt{\Gamma t}$.

Results: Late-time evolution of the interface



From dimensional analysis, we expect a purely circulation growth of the interface perturbation to behave according to $a(t) \sim \sqrt{\Gamma t}$.

Results: Dependence of interface dynamics on wave duration



- Changing wave width changes time when expansion hits interface.
- Time-dependent interface deformation causes time-dependent vorticity deposition.
- The long-term interface dynamics can change appreciably.

Order of magnitude analysis of vorticity generation

$$\frac{\partial \vec{\omega}}{\partial t} + (\vec{u} \cdot \nabla) \vec{\omega} = -\vec{\omega} (\nabla \cdot \vec{u}) + \frac{\nabla \rho \times \nabla p}{\rho^2}.$$

Order of magnitude analysis of vorticity generation

$$\frac{\partial \vec{\omega}}{\partial t} + (\vec{u} \cdot \nabla) \vec{\omega} = -\vec{\omega} (\nabla \cdot \vec{u}) + \frac{\nabla \rho \times \nabla p}{\rho^2}.$$

Acoustic Relations and operator treatments

$$\Delta p_a = \pm \Delta u_a \rho c = c^2 \Delta \rho_a, \quad \|\nabla f\| \sim \|\nabla \cdot f\| \sim \|\nabla \times f\| = \mathcal{O}(|\Delta f| / \Delta L)$$

Order of magnitude analysis of vorticity generation

$$\frac{\partial \vec{\omega}}{\partial t} + (\vec{u} \cdot \nabla) \vec{\omega} = -\vec{\omega} (\nabla \cdot \vec{u}) + \frac{\nabla \rho \times \nabla p}{\rho^2}.$$

Acoustic Relations and operator treatments

$$\Delta p_a = \pm \Delta u_a \rho c = c^2 \Delta \rho_a, \quad \|\nabla f\| \sim \|\nabla \cdot f\| \sim \|\nabla \times f\| = \mathcal{O}(|\Delta f| / \Delta L)$$

Baroclinic vorticity generation

$$\left\| \frac{\nabla \rho \times \nabla p}{\rho^2} \right\| = \mathcal{O} \left(\frac{|\Delta \rho_I| |\Delta p_a|}{|\Delta L_I| |\Delta L_a|} \frac{1}{|\rho|^2} |\theta| \right)$$

Order of magnitude analysis of vorticity generation

$$\frac{\partial \vec{\omega}}{\partial t} + (\vec{u} \cdot \nabla) \vec{\omega} = -\vec{\omega} (\nabla \cdot \vec{u}) + \frac{\nabla \rho \times \nabla p}{\rho^2}.$$

Acoustic Relations and operator treatments

$$\Delta p_a = \pm \Delta u_a \rho c = c^2 \Delta \rho_a, \quad \|\nabla f\| \sim \|\nabla \cdot f\| \sim \|\nabla \times f\| = \mathcal{O}(|\Delta f| / \Delta L)$$

Baroclinic vorticity generation

$$\left\| \frac{\nabla \rho \times \nabla p}{\rho^2} \right\| = \mathcal{O} \left(\frac{|\Delta \rho_I| |\Delta p_a|}{|\Delta L_I| |\Delta L_a|} \frac{1}{|\rho|^2} |\theta| \right)$$

Advective and compressible vorticity generation - $\|\vec{\omega}\| = \int_0^{\Delta t_a} (\text{baroclinic term}) dt$

$$\|(\vec{u} \cdot \nabla) \vec{\omega}\| \sim \|-\vec{\omega} (\nabla \cdot \vec{u})\| = \mathcal{O} \left(\left[\frac{|\Delta u_a|}{|\Delta L_a|} \right]^2 \right),$$

Order of magnitude analysis of vorticity generation

$$\frac{\partial \vec{\omega}}{\partial t} + (\vec{u} \cdot \nabla) \vec{\omega} = -\vec{\omega} (\nabla \cdot \vec{u}) + \frac{\nabla \rho \times \nabla p}{\rho^2}.$$

Acoustic Relations and operator treatments

$$\Delta p_a = \pm \Delta u_a \rho c = c^2 \Delta \rho_a, \quad \|\nabla f\| \sim \|\nabla \cdot f\| \sim \|\nabla \times f\| = \mathcal{O}(|\Delta f| / \Delta L)$$

Baroclinic vorticity generation

$$\left\| \frac{\nabla \rho \times \nabla p}{\rho^2} \right\| = \mathcal{O} \left(\frac{|\Delta \rho_I| |\Delta p_a|}{|\Delta L_I| |\Delta L_a|} \frac{1}{|\rho|^2} |\theta| \right)$$

Advective and compressible vorticity generation - $\|\vec{\omega}\| = \int_0^{\Delta t_a} (\text{baroclinic term}) dt$

$$\|(\vec{u} \cdot \nabla) \vec{\omega}\| \sim \|-\vec{\omega} (\nabla \cdot \vec{u})\| = \mathcal{O} \left(\left[\frac{|\Delta u_a|}{|\Delta L_a|} \right]^2 \right),$$

Comparing terms for our problem

$$\Delta t_a \approx 5\lambda/c_w, \quad \Delta L_a = 5\lambda, \quad \Delta p_a = 10 \text{ MPa}, \quad \Delta L_I \approx 0.05\lambda, \quad <|\theta|> = 0.12$$

$$\frac{\left\| \frac{\nabla \rho \times \nabla p}{\rho^2} \right\|}{\|-\vec{\omega} (\nabla \cdot \vec{u})\|} = \frac{c}{|\Delta u_a|} = \frac{\rho}{|\Delta \rho_a|} = \mathcal{O}(10^2)$$

Order of magnitude analysis of vorticity generation

$$\frac{\partial \vec{\omega}}{\partial t} + (\vec{u} \cdot \nabla) \vec{\omega} = -\vec{\omega} (\nabla \cdot \vec{u}) + \frac{\nabla \rho \times \nabla p}{\rho^2}.$$

Acoustic Relations and operator treatments

$$\Delta p_a = \pm \Delta u_a \rho c = c^2 \Delta \rho_a, \quad \|\nabla f\| \sim \|\nabla \cdot f\| \sim \|\nabla \times f\| = \mathcal{O}(|\Delta f| / \Delta L)$$

Baroclinic vorticity generation

$$\left\| \frac{\nabla \rho \times \nabla p}{\rho^2} \right\| = \mathcal{O} \left(\frac{|\Delta \rho_I| |\Delta p_a|}{|\Delta L_I| |\Delta L_a|} \frac{1}{|\rho|^2} |\theta| \right)$$

Advective and compressible vorticity generation - $\|\vec{\omega}\| = \int_0^{\Delta t_a} (\text{baroclinic term}) dt$

$$\|(\vec{u} \cdot \nabla) \vec{\omega}\| \sim \|-\vec{\omega} (\nabla \cdot \vec{u})\| = \mathcal{O} \left(\left[\frac{|\Delta u_a|}{|\Delta L_a|} \right]^2 \right),$$

Comparing terms for our problem

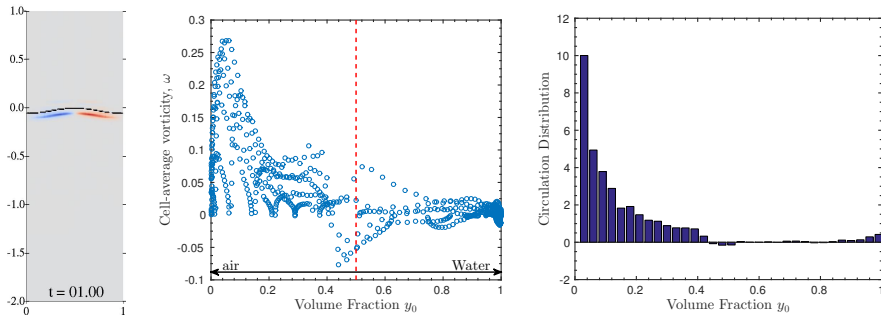
$$\Delta t_a \approx 5\lambda/c_w, \quad \Delta L_a = 5\lambda, \quad \Delta p_a = 10 \text{ MPa}, \quad \Delta L_I \approx 0.05\lambda, \quad <|\theta|> = 0.12$$

$$\frac{\left\| \frac{\nabla \rho \times \nabla p}{\rho^2} \right\|}{\|-\vec{\omega} (\nabla \cdot \vec{u})\|} = \frac{c}{|\Delta u_a|} = \frac{\rho}{|\Delta \rho_a|} = \mathcal{O}(10^2)$$

Calculated values at $t = 1$:

$$\int \frac{\nabla \rho \times \nabla p}{\rho^2} dA = 7.7 \text{e-}3, \quad \int (\vec{u} \cdot \nabla) \vec{\omega} dA = -5.3 \text{e-}5, \quad \int -\vec{\omega} (\nabla \cdot \vec{u}) dA = 2.7 \text{e-}5,$$

Vorticity generation occurs predominately in gas-dominated fluid

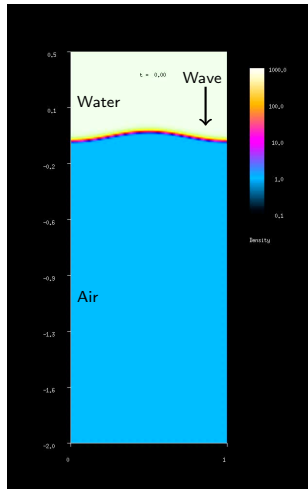
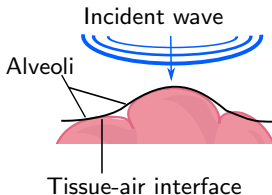
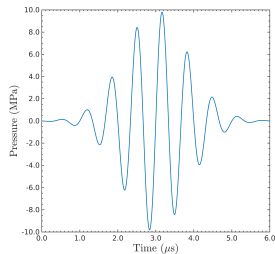


$$\frac{\left\| \frac{\nabla \rho \times \nabla p}{\rho^2} \right\|_{air}}{\left\| \frac{\nabla \rho \times \nabla p}{\rho^2} \right\|_{water}} = \mathcal{O} \left(|\mathbf{T}| \left(\frac{|\rho^-|}{|\rho^+|} \right)^2 \right) \approx 357, \quad (*)$$

$$\mathbf{T} = \frac{2(\rho c)_{air}}{(\rho c)_{air} + (\rho c)_{water}}$$

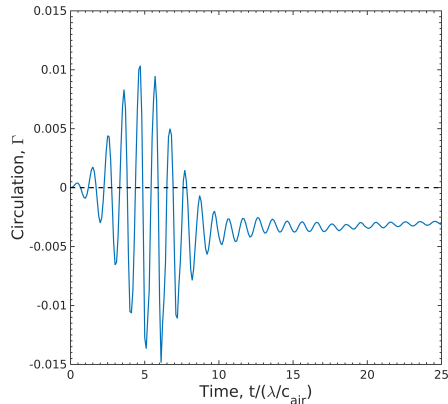
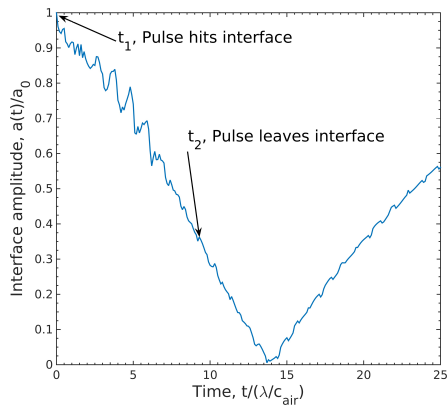
- 97% of circulation appears in fluid with $y_0 < 0.5$
- Computed ratio of circulation in gas-dominated fluid ($y_0 < 0.5$) to liquid-dominated fluid ($y_0 > 0.5$), $\int(*)dA = \mathcal{O}(10^1)$

We simulated and US-pulse impinging on a water-air interface



- Qualitatively this looks like the interface for the trapezoidal wave.
- Longer simulations are needed to check late-time behavior.

Interface response to a 10 MPa US pulse



- Qualitatively, the interface response for the 10 MPa US pulse looks very similar to the 10 MPa trapezoidal wave.
- The circulation deposited is of the same order as the equivalent amplitude trapezoidal wave.

Summary and conclusions thus far

Summary:

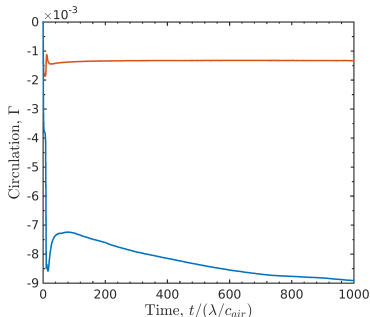
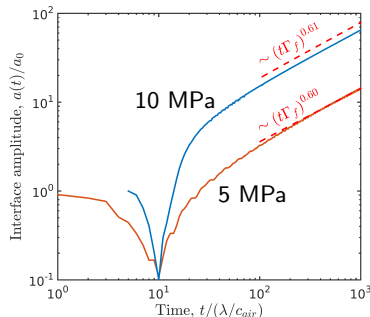
- I studied the interaction of finite-duration acoustic waves with gas-liquid interfaces.

Conclusions

- Baroclinic vorticity generated by wave-interface interaction is likely capable of deforming perturbed liquid-gas interfaces.
- Circulation remaining after the wave determines the long term dynamics.
- Circulation deposition depends on interface morphology.
- Changes in the acoustic waveform that have little affect on the interface during the wave-interface interaction can substantially affect post-wave interface dynamics, via vorticity.
- Baroclinic vorticity is deposited at the interface, predominantly in gas-dominated ($y_0 < 0.5$) fluids.
- Interface responses are qualitatively similar for trapezoidal and US waves.

Part III: Future work

I aim to further our understanding of the relevant fluid mechanics

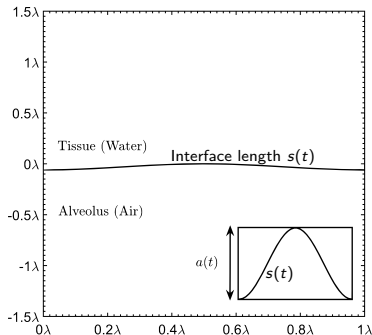


- Explain the discrepancies between numerical results and $a(t) \sim \sqrt{\Gamma t}$
- Develop a model and scaling law for circulation $\Gamma(\nabla p, a_0)$ deposited on a slightly perturbed interface by a compression or expansion wave
- Invert the waves to confirm counter rotating vortices relevant growth

I plan to increase the relevance to DUS

Hypothesis: Baroclinic vorticity drives deformation to the point of stress or strain failure in pulmonary capillaries.

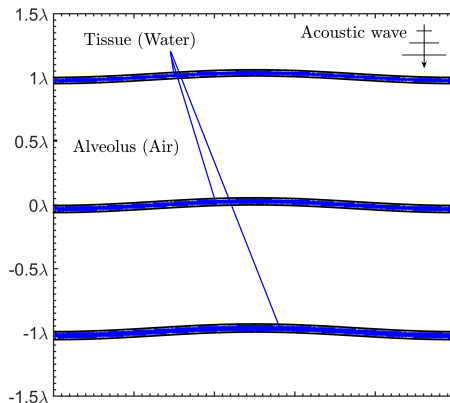
- Rabbit pulmonary capillaries have been shown to hemorrhage at transmural stresses of ≈ 5 kPa (West *et al.*, 1991).
- I will calculate elastic and (passive) viscous stresses at the interface.



I plan to increase the relevance to DUS

Hypothesis: vorticity induced deformation and subsequent hemorrhage will allow acoustic waves and hemorrhage to propagate into subsequent layers of alveoli

- Damage exists in clearly defined hemorrhage area, not behind it (Penney *et al.*, 1993).
- Propagation mechanism of US-induced lesions are unknown (Zachary *et al.*, 2006).



Future work (beyond me)

To fully understand the role that fluid mechanics plays in DUS-induced lung hemorrhage, the following problems need to be addressed:

- Viscous effects
- Elasticity and failure mechanics
- Multiple pulses (via time-dependent boundary conditions)
- Detailed pulmonary structure

- Beyer, Robert T. 1974. *Nonlinear Acoustics*.
- Brouillette, Martin. 2002. The Richtmyer-Meshkov Instability. *Annual review of fluid mechanics*, **34**(1), 445–468.
- Child, S.Z., Hartman, C.L., Schery, L.A., & Carstensen, E.L. 1990. Lung damage from exposure to pulsed ultrasound. *Ultrasound in medicine & biology*, **16**(8), 817–825.
- Drake, Paul. 2006. *High-Energy-Density Physics*. Shock Wave and High Pressure Phenomena. Springer Berlin Heidelberg.
- Heifetz, E., & Mak, J. 2015. Stratified shear flow instabilities in the non-Boussinesq regime. *Physics of fluids*, **27**(8), 086601.
- Miller, DL. 2012. Induction of Pulmonary Hemorrhage in Rats During Diagnostic Ultrasound. *Ultrasound in medicine & biology*, **38**(8), 1476–1482.
- Miller, Douglas L., Dou, Chunyan, & Wiggins, Roger C. 2008. Frequency Dependence of Kidney Injury Induced by Contrast-Aided Diagnostic Ultrasound in Rats. *Ultrasound in medicine and biology*, **34**(10), 1678–1687.
- O'Brien, William D. W.D., & Zachary, J.F. 1997. Lung damage assessment from exposure to pulsed-wave ultrasound in the rabbit,

mouse, and pig. *ieee transactions on ultrasonics, ferroelectrics and frequency control*, **44**(2), 473–485.

Penney, D.P., Schenk, E.A., Maltby, K., Hartman-Raeman, C., Child, S.Z., & Carstensen, E.L. 1993. Morphological effects of pulsed ultrasound in the lung. *Ultrasound in medicine & biology*, **19**(2), 127–135.

Tarantal, Alice F., & Canfield, Don R. 1994. Ultrasound-induced lung hemorrhage in the monkey. *Ultrasound in medicine & biology*, **20**(1), 65–72.

Wei, Kevin, Le, Elizabeth, Bin, Jian-Ping, Coggins, Matthew, Thorpe, Jerrel, & Kaul, Sanjiv. 2001. Quantification of renal blood flow with contrast-enhanced ultrasound. *Journal of the american college of cardiology*, **37**(4), 1135–1140.

West, J B, Tsukimoto, K, Mathieu-Costello, O, & Prediletto, R. 1991. Stress failure in pulmonary capillaries. *Journal of applied physiology (bethesda, md. : 1985)*, **70**(4), 1731–1742.

Zachary, James F., Blue, James P., Miller, Rita J., Ricconi, Brian J., Eden, J. Gary, & O'Brien, William D. 2006. Lesions of ultrasound-induced lung hemorrhage are not consistent with thermal injury. *Ultrasound in medicine and biology*, **32**(11), 1763–1770.

BACKUP SLIDES

Argument against viscosity - viscous length scales

$$\nu_w = 0.7 \mu\text{m}^2/\text{s}, \quad \nu_a = 16.6 \mu\text{m}^2/\text{s}, \quad f_c = \mathcal{O}(10^6) \text{ Hz}$$

$$\sqrt{\nu_{air}/f_c} = 4\mu \text{ m} = \mathcal{O}(10^{-6}) \ll L_{alveolus} = \mathcal{O}(10^{-4})$$

$$\sqrt{\nu_{air,ND} t} \approx 0.5 < a(t) - a_0 \approx 4 \text{ at } t = 1000$$

Therefore the scale of the viscous effect is smaller than the scale of the problem we are looking at, but may be important at late times.

Dimensional Numbers

- Let $\lambda_{alveolus} = 100\mu \text{ m}$, $u_0 = c_{air} = 343 \text{ m}$, $v_0 = \langle a(t) \rangle \approx 0.65 \text{ m/s}$,
 $u_{intf}(t=20) = 12.8 \text{ m/s}$, $G = 1 \text{ kPa}$
- $\lambda_{alveolus} = 100\mu \text{ m}$, $u_0 = c_{air} = 343 \text{ m}$, $v_0 = \langle a(t) \rangle \approx 0.65 \text{ m/s}$
- $t = 1 \rightarrow t_{dim} = 0.292\mu \text{ s}$

Dimensionless Numbers

- $Fr = \frac{u_0}{\sqrt{g_0 \lambda}} \approx 11000$
- $Fr = \frac{v_0}{\sqrt{g_0 \lambda}} \approx 21$
- $Ca = \frac{\rho u_{intf}^2}{G_{Alv}} = 163$

Interface treatment

Interface thickness parameter:

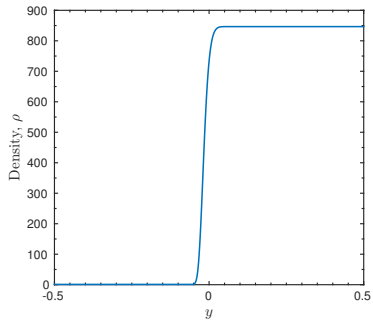
$$\delta = 0.08\lambda$$

Normalized distance from interface:

$$d = \frac{\delta + y(x)_{interface} - y}{2\delta}$$

Volume fraction:

$$y_0 = \begin{cases} 1 \\ \exp \left(\log (10^{-16}) |d|^8 \right) \\ 0 \end{cases}$$



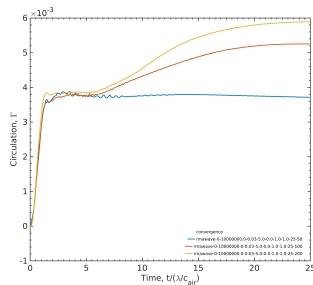
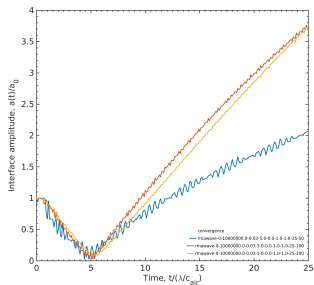
Radiation Pressure

$$P_{net} = \frac{\Delta p_a}{2} \left[1 - \frac{c_w}{c_a} + \frac{(\rho c)_a - (\rho c)_w}{(\rho c)_a (\rho c)_w} \right] \text{ Beyer (1974)}$$

Stress failure in the lungs:

Rabbit lungs under transmural pressure: $\approx 5.2 \text{ kPa}$ (West *et al.*, 1991);

Convergence tests: Compression wave



50 pts / λ ,

100 pts / λ

200 pts / λ